Int J Clin Exp Med 2019;12(12):13288-13297
www.ijcem.com /ISSN:1940-5901/IJCEM0099107

*Original Article*

# Infrared thermal imaging analysis of the human abdomen based on convolution neural network optimized by a genetic algorithm

Di Ma[1], Zichen Lu[2], Longlong Liu[1], Xiaoyan Lu[3]

*[1]School of Mathematical Sciences, Ocean University of China, Qingdao 266000, P. R. China; [2]Cloud Computing Center, Chinese Academy of Science, Dongguan 523000, P. R. China; [3]Dongguan Hospital of Traditional Chinese Medicine, Dongguan 523000, P. R. China*

Received July 1, 2019; Accepted October 9, 2019; Epub December 15, 2019; Published December 30, 2019

**Abstract:** In order to find an efficient and accurate method to analyze infrared thermography images, this paper innovatively combines a genetic algorithm with a convolutional neural network to construct a convolution neural network model (GA-CNN), which provides the basis of a diagnostic tool for doctors, also saving valuable time for patients. Using genetic algorithm initialization, the GA-CNN model can be used to find the optimal network structure, thus avoiding the influence of random initialization of traditional neural network weights. The genetic algorithm can improve the accuracy of the network through optimization of the convolution core content, convolution core size, convolution core number, pooling mode, pooling layer size and other structural parameters of convolution neural network. Real infrared thermography images from a Chinese medicine hospital were taken as samples for the model in order to detect illness in human abdomens through classification of the infrared thermography images. The excellent performance of the model proposed in this paper offers direct improvement of the prediction accuracy to 92.96%. Therefore, the GA-CNN model proposed in this paper is a very effective infrared thermal imaging analysis method, which can provide a reliable basis for the diagnosis of abdominal diseases.

**Keywords:** Convolutional neural network, infrared thermal imaging, genetic algorithm

## Introduction

Infrared thermal imaging technology plays an important role in Traditional Chinese Medicine research as a visualization and objectification technology, as it is a non-invasive method that does not require radiation with wide applicability in assisting doctors to diagnose patients [1, 2]. Thus, it has been widely been used in various aspects of medical research [3]. Analysis of infrared thermograms has the potential to be used by doctors as a basis for disease diagnosis [4]. Denoble [5] predicted the severity of knee arthritis based on the differences in average temperature and the standard deviation between infrared thermal imaging images of knee joints, and objectively proved the reliability of infrared thermal imaging technology. Kacmaz [6] proved that infrared thermal imaging could be used as an effective method for the diagnosis of deep venous thrombosis by using computer-aided software. Calin and others [7] suggested that thermal infrared imaging could be effective in the diagnosis, evaluation and monitoring of knee joint lesions, and could be used as an adjunct method to conventional medicine. Shih and others [8] confirmed that DITI (Digital infrared thermal imaging) could be used reflect the degree of orbital inflammation. Vardasca and Simoes [9] found that thermal imaging was an effective way of detecting breast cancer, with a sensitivity of up to 100%. Mie Jin and others [10] proved that skin temperature measurement of hands and feet by digital thermography is useful for diagnosis of Raynaud's phenomenon. Infrared thermal imaging technology has broad application prospects in traditional Chinese medicine treatment [11, 12]. However, extensive promotion of this technology is difficult due to a lack of professionals in the field of infrared thermal imaging detection [13-15]. At the same time, significant

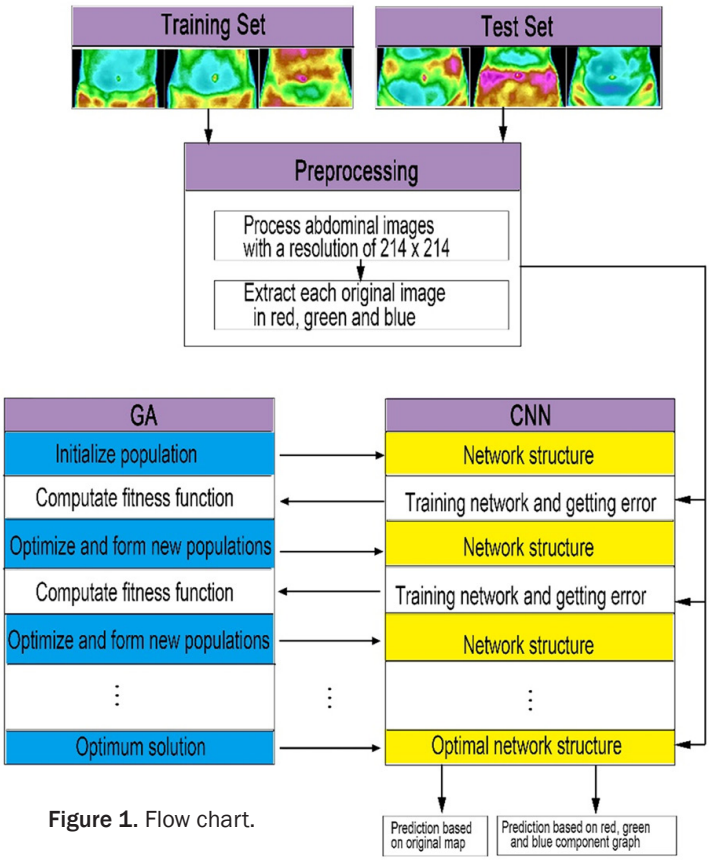


**Figure 1.** Flow chart.

time and effort is required for analysis of a large number of infrared thermal images [16], which is an urgent problem that needs to be solved.

Previous related research has combined machine learning, artificial neural networks and infrared thermal imaging technology and applied these methods to pattern recognition. Liu and her students [17-20] applied an artificial neural network and deep learning technology to the recognition and prediction of biological information and achieved good results. Other scholars have applied neural networks and infrared thermal imaging technology to the diagnosis of diseases. As early as 1979, scholars suggested that thermography was superior to mammography for breast cancer screening [21] and related research in recent years has continued to support this theory. Jung, Hsieh and Chen [22] built a database that could be used to detect breast diseases using infrared images. Lessa [23] used an artificial neural network and biological statistics to analyze mammary thermograms in order to diagnose breast cancer with an accuracy of 80.95%. Silva [24] classified mammograms based on thermal imaging technology by using an artificial neural network non-linear classification model, which was shown to have an accuracy rate for breast cancer classification of 85%. Koay [25] trained a simple artificial neural network to predict the occurrence of breast cancer based on statistical differences in mean temperature and standard deviation. Jin and others [26] evaluated an infrared thermal imaging system for carpal tunnel syndrome diagnosis by means of an artificial neural network and proved its feasibility.

This study identifies and preliminarily judges a thermogram using the strong learning and prediction ability of an artificial neural network and provides a reliable basis for clinical diagnosis, which can save both doctors' and patients' time.

## Methods

This paper constructs a genetic algorithm-optimized convolutional neural network model (GA-CNN) and finds an optimal network structure by learning the infrared thermal images of the human abdomen in order to explore an efficient and convenient method for abdominal disease diagnosis. The algorithm flow used in this paper is shown in **Figure 1** and can be described as follows.

*Convolutional neural networks (CNN)*

A convolutional neural network is a type of multi-layer neural network which can realize automatic feature learning. Compared with traditional recognition algorithms, this model offers many advantages for large-scale image recognition and classification, due to its low complexity, low number of weight values, weight sharing and ability to avoid a complex manual extraction process. In this paper, a five-layer convolution neural network is constructed (**Figure 2**).

In the input layer, the input $X$ of the network is usually an image, and the pixel values of the image form a matrix.

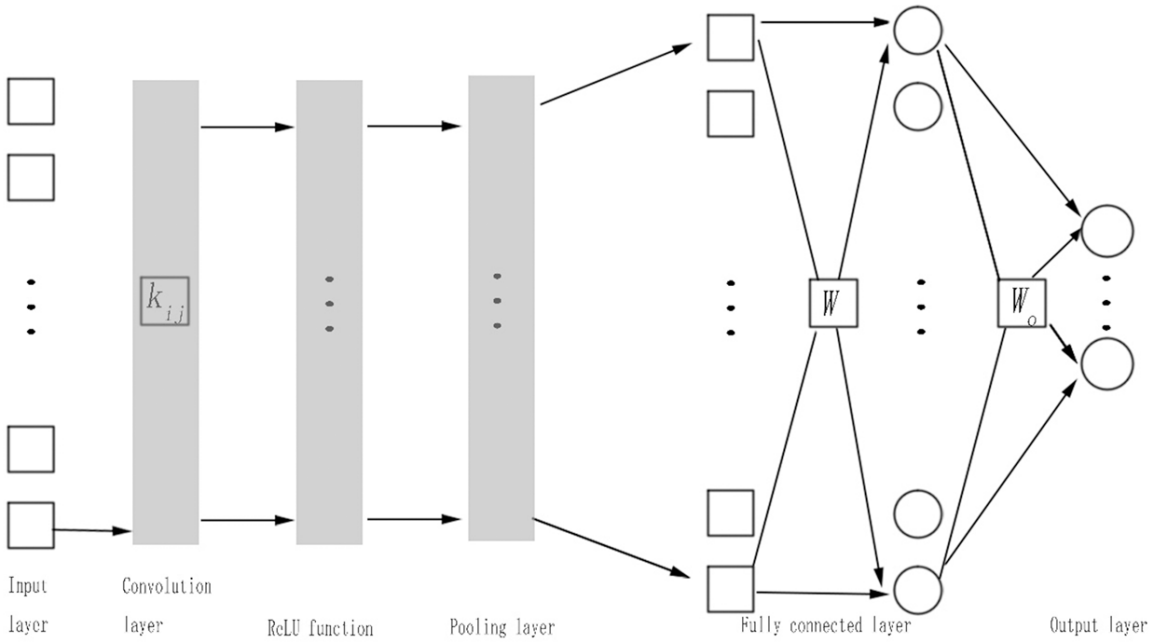


**Figure 2.** The structure of CNN.

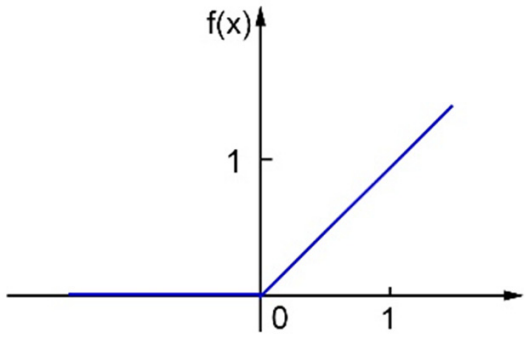


**Figure 3.** The function of ReLU.

In the convolution layer, the input sample is convoluted with a learnable convolution core. Different features can be extracted by convolution of the different convolution kernels. The feature maps of these different features can be used together as the input data for the pooling layer.

The $j$th feature map $a_j^1$ of the output in the convolution layer is as follows:

$$a_j^1 = f\left(b_j + \sum_{i \in M_j} x_i * k_{ij}\right) \quad (1)$$

Where $f(\cdot)$ is the activation function, $b_j$ is the $j$th bias, $x_i$ is the $i$th pixel value of the input layer, * is the convolution operation, $k_{ij}$ is the convolution core and $M_j$ is a subset of the input feature graph.

The activation function $f(\cdot)$ of convolution layer mapped the convoluted value to the value with a specific boundary. The common activation functions were Sigmoid, Tanh, ReLU, etc. This paper chose ReLU function (**Figure 3**).

In the pooling layer, the feature map of the upper layer is downsampled. Many pixels are compressed into a single feature that forms a new feature map. The $j$th feature map $a_j^2$ output from the pooling layer is as follows:

$$a_j^2 = pooling(a_j^1) \quad (2)$$

Where *pooling* denotes the pooling operation that divides the feature map $a_j^1$ into several rectangular image blocks of the same size without overlap, and operates on the pixels in each image block. Common pooling methods used include maximum pooling (the maximum pixel value in the image block is taken as the pixel for the new feature point) and average pooling (the average value of the pixel in the image block is taken as the pixel for the new feature point).

In the full connection layer, the pooled feature map is transformed into a series of nodes to form a feature vector $x$ which connects all the neurons in the full connection layer and serves as the input to the full connection layer. After operating the activation function $f(\cdot)$, the feature map is output to the output layer. The vec-

tor $Y$ is composed of the output values of the neurons in the full connection layer which is as follows:

$$Y = f(W \cdot X) \tag{3}$$

Where $W$ is the connection weight matrix of the full connection layer and the activation function $f(\cdot)$ of the hidden layer is chosen to be the ReLU function.

The Softmax function is chosen as the activation function $f(\cdot)$ of the neurons in the output layer. The output value of the neuron constitutes a vector $Z$:

$$Z = f(W_o \cdot Y) \tag{4}$$

Where $W_o$ is the connection weight matrix of the output layer.

*GA-CNN*

The genetic algorithm is an algorithm that encodes the parameters of the problem into chromosomes in order to mimic biological evolution. Chromosome information is exchanged by means of selection, crossover and mutation within the population. After mutiple iterations, the optimal individual (chromosome) will be finally obtained.

Individuals are composed based on the convolution core content, size, number, pooling mode, pooling layer size and other structural parameters of the convolution neural network. N individuals are randomly selected to form a population. The initial population is used as the parent generation, and the corresponding fitness values of each individual are calculated. Individuals that satisfy certain conditions are obtained by iterative evolution to be the optimal network parameters.

The specific operation steps used are as follows:

*1) Mapping objective function to fitness function:*

The following fitness function is selected, and the fitness $F$ of the neural network is:

$$F = 1/(E+\varepsilon) \tag{5}$$

ε should be a very small positive number to ensure that the molecule is not zero, and was set as 0.001 here. The objective function $E$ is the sum of the squares of errors between the real value $y_i$ and the predicted value $O_i$ of the output of the neural network:

$$E = \sum_{i=1}^{N} (y_i - o_i)^2 \tag{6}$$

*2) Encoding and establishing the initial population:*

In this paper, a real-number coding method is used. $C,X_c*X_c,N_c,P,X_P*X_P$ denote the content, size, number of convolution cores, pooling method and the size of the pooling layer, respectively. The gene sequence of an individual can then be expressed as:

$$X_i = [C, X_c, N_c, P, X_p] \tag{7}$$

The initial population is generated randomly as $M = \{X_1, X_2, ..., X_N\}$ where $X_i \in M$ ($i$ = 1, 2,...$N$) is an individual in the initial population.

*3) The maximum number of cycles of the algorithm is set as 500 and the optimal fitness value is set as 0.98:*

*4) Calculation of fitness function:*

The fitness values of all individuals in generation $t$ are calculated according to the fitness function. Step 7) is executed when the optimal fitness value or the maximum number of cycles is reached, otherwise, step 5) is executed.

*5) Genetic operation:*

① Selection operation

The fitness ratio method is used for selection. If the population size is $n$ and the fitness of an individual $i$ is $f_i$, the probability $P_{si}$ of $i$ being selected is:

$$P_{si} = f_i / \sum_{i=1}^{n} f_i \tag{8}$$

② Crossover operation

Arithmetic crossover generates two new individuals, which are set between $x_A^t$ and $x_B^t$ to perform the arithmetic crossover. The new individuals are:

$$\begin{cases} x_A^{t+1} = \alpha x_B^t + (1 - \alpha) x_A^t \\ x_B^{t+1} = \alpha x_A^t + (1 - \alpha) x_B^t \end{cases} \tag{9}$$

Where $\alpha$ is a random number uniformly distributed in the interval [0, 1].

③ Mutation operation

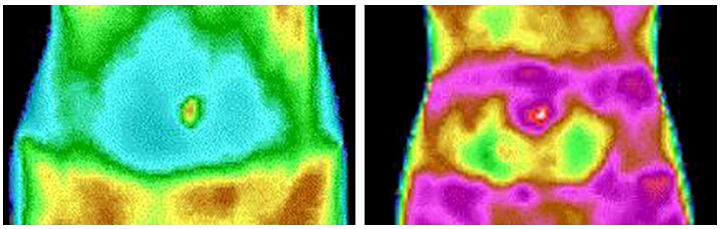

**Figure 4.** Positive sample image (left) and negative sample image (right).

A variable $x_i$ is randomly selected according to a certain variation rate and mutates into a uniform random number $r$ in $[a_i, b_i]$. The new individual is obtained as follows:

$$x_i' = \begin{cases} r \text{ if } i = j \\ x_i \text{ if } i \neq j \end{cases}, j \in \{1, 2, \text{L } n\}, \text{Uniform random selection} \quad (10)$$

*6) Generating a new generation of individuals:*

After genetic manipulation, the next generation of individuals is generated, and step 4) is then repeated.

*7) Termination:*

Once the best individual output is obtained, the loop is terminated and the optimal network structure is obtained.

*Application results of GA-CNN*

Infrared thermography has a high application potential as a diagnostic method for scientific and medical research. With traditional diagnostic methods, doctors must analyze and diagnose images individually, which can lead to delays in diagnosis for patients seeking medical advice. In order to address this problem, this paper aims to provide a diagnostic basis for doctors by applying the GA-CNN model constructed here.

Different color levels on an infrared thermal image represent different temperature zones, i.e. white represents a high heat zone, red represents a hot zone, yellow represents a temperature zone, while green, blue and purple represent cool, cold and super cold zones, respectively. The surface temperature of a local body will change with the occurrence of abdominal abnormalities and thus by analyzing abnormal temperature changes, doctors can make a diagnosis in conjunction with the patients' medical history, physical condition and other factors.

*Sources of data*

The data samples used were provided by a Chinese medicine hospital in Guangdong Province, China. Patient consent was obtained for all images and personal information was removed. Additionally, all subjects were subject to the ethical standards established by the related institution. The sample set consisted of 250 infrared thermal images of healthy abdomens (negative samples) and 250 infrared thermal images of abdominal diseases such as ovarian diseases, uterine diseases, appendicitis and cystitis (positive samples). As shown in **Figure 4**, the thermal imaging color distribution of negative samples is symmetrical, with the lowest temperature shown in blue in the middle of the abdomen, surrounded by slightly higher temperatures with a small amount of green, and higher temperatures shown in red and yellow in the lower abdomen. The color distribution of the positive sample images has no obvious symmetry, and the color may appear yellow or red because of the high temperatures. All external factors were excluded when the thermograms were taken, in order to ensure that the samples were taken at the same temperature, at the same shooting distance and in a resting state. For these images, the sample labels on the abdominal diseases was determined by authoritative doctors after examination. Some samples are shown in **Figure 4**.

*Data preproccessing*

In order to obtain uniform samples, 500 color RGB images were cut and processed into human abdominal images of 134*214*3 pixels, denoted as data set *D*.

*Operation and results*

*Recognition and prediction of color images:* First, an optimal network structure was obtained using a 7-fold cross-test method with 428 images (214 positive samples and 214 negative samples) as the training sets to teach the network. The network was then tested using a test set consisting of 72 images (36 positive samples and 36 negative samples). Finally, the testing results were compared with

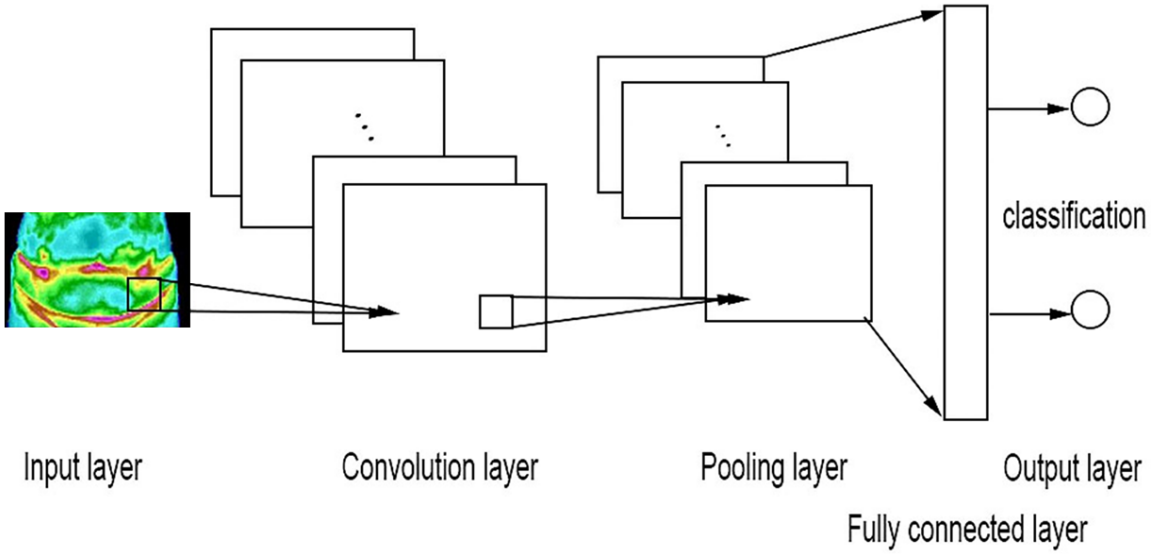


**Figure 5.** Image recognition and prediction based on GA-CNN model.

**Table 1.** Model running results when inputting color maps

| Convolution Kernel Size | No. of Convolution Kernels | Pooling Layer Mode | Pooling Layer Size |
|---|---|---|---|
| 3×3 | 23 | Average pooling | 2×2 |

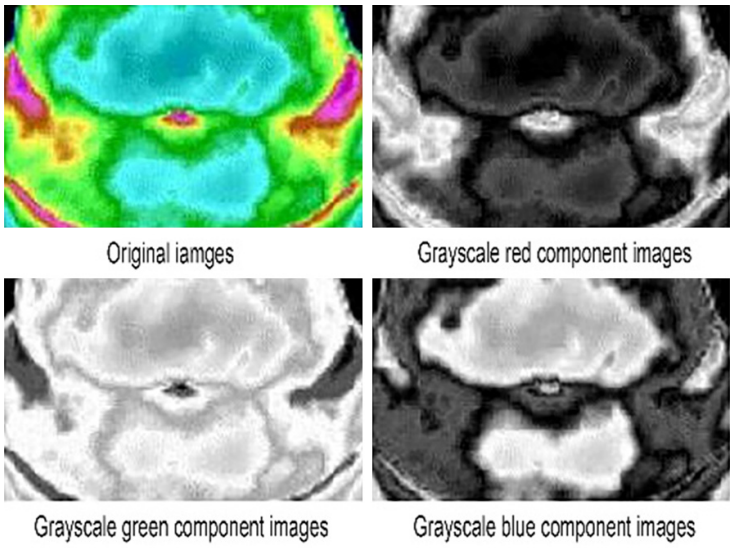


**Figure 6.** Gray-scale image after extracting each component and the original image.

the known results, using the following formula and obtaining an average accuracy $a$ over seven calculations to obtain the prediction accuracy of the model:

$$a = \frac{1}{7}\sum(N_c/N_t) \quad (11)$$

In the formula, $N_c$ represents the correct number of predictions and $N_t$ represents the total number of test sets.

The network structure is shown in **Figure 5**. The number of nodes in the hidden layer is 100, the initial population is 200, the maximum number of cycles is 500 and the variation rate is 0.1. The results shown in **Table 1** show that the network prediction accuracy is 80.28%, which is not ideal.

*Recognition and prediction of gray image*

As image recognition of color images can be difficult, in order to obtain a higher prediction accuracy, we decided to extract the red, green and blue components of the RGB color image separately and converted them to grayscale. After each operation, three images were generated for each color image (resolution 134 * 214 * 1) (**Figure 6**). Five hundred grayscale red component images formed the database $D_r$, 500 grayscale green component images formed the database $D_g$ and 500 grayscale blue component images formed the database $D_b$.

**Table 2.** The results of model operation when Inputting gray scale image

| Convolution Kernel Size | No. of Convolution Kernels | Pooling Layer Mode | Pooling Layer Size |
|---|---|---|---|
| 5×5 | 20 | Average pooling | 2×2 |

Using the same parameters and the weight initialization method as described previously, the GA-CNN model was used with databases $D_r$, $D_g$ and $D_b$ to obtain the predicted value using the 7-fold cross-test. If different grayscale databases gave inconsistent prediction results for the same color image, the two prediction results with the same value were taken as the final result. The results shown in **Table 2** show that the accuracy of the network testing is increased to 92.96%.

These results suggest that the GA-CNN model proposed in this paper can optimize the traditional CNN method by using optimal network parameters to recognize and predict the image, and achieves a satisfactory prediction accuracy.

The output images of different layers during the GN-CNN model processing are shown in **Figure 7**, taking the R component gray scale image of a patient's infrared thermal imaging image as an example.

The feature layer extraction of the convolution neural network optimized by the genetic algorithm is composed of an alternate convolution layer and a pooling layer. By using the convolution filter, the image generated by the convolution layer highlights the features of the input image and the optimized pooling layer can effectively reduce the size of the image without changing the original image, thus reducing the required computational resources.

*Model assessment*

The performance of the GA-CNN model was further evaluated for the two databases mentioned above by adopting three models: GA-CNN, CNN and DCNN (Deep Convolution Neural Network), to predict the image (**Table 3**).

The results show that the GA-CNN model proposed in this paper has the highest prediction accuracy. This is due to the optimized initial parameter values, such as the convolution core and the size of the pooling layer of the neural network by the genetic algorithm, which avoids the influence of random initialization of the weights using in a traditional neural network.

## Discussion

Due to the existence of a convolution layer and a pooling layer, a convolution neural network has a higher accuracy for image recognition than other neural networks. However, the GA-CNN model proposed in this paper optimizes the convolution neural network parameters to obtain an even higher prediction accuracy than a deep convolution neural network that uses a random selection of common parameters. This is shown to be an effective improvement of the convolution neural network.

The GA-CNN model proposed in this paper was applied to the recognition and classification of real human abdominal infrared thermal imaging, with satisfactory accuracy. The accuracy was higher than an ordinary CNN model and DLCNN model for both the color image data sets and the grayscale image data sets. This further verifies the validity and superiority of this model.

However, there were some unfavorable factors that caused interference in the model presented in this paper, which affected the overall accuracy:

1) Infrared thermal imaging technology represents only the body surface temperature. However, changes in body surface temperature can occur due to reasons other than pathological changes in the body, such as short-term external interference or skin dysfunction. 2) The judgment on whether a patient is ill or not (i.e. the sample label) was provided by an expert with the help of professional knowledge. However, the expert's judgment may not be entirely correct, i.e., there may be errors in our learning samples. 3) Infrared equipment itself has some limitations, as interference can occur due to many factors. The shooting distance and the shooting environment temperature will lead to the appearance of a pseudo-heterothermal zone, which will also lead to inaccurate judgment results to a certain extent.

As more data samples are collected, we can further verify the performance of the model

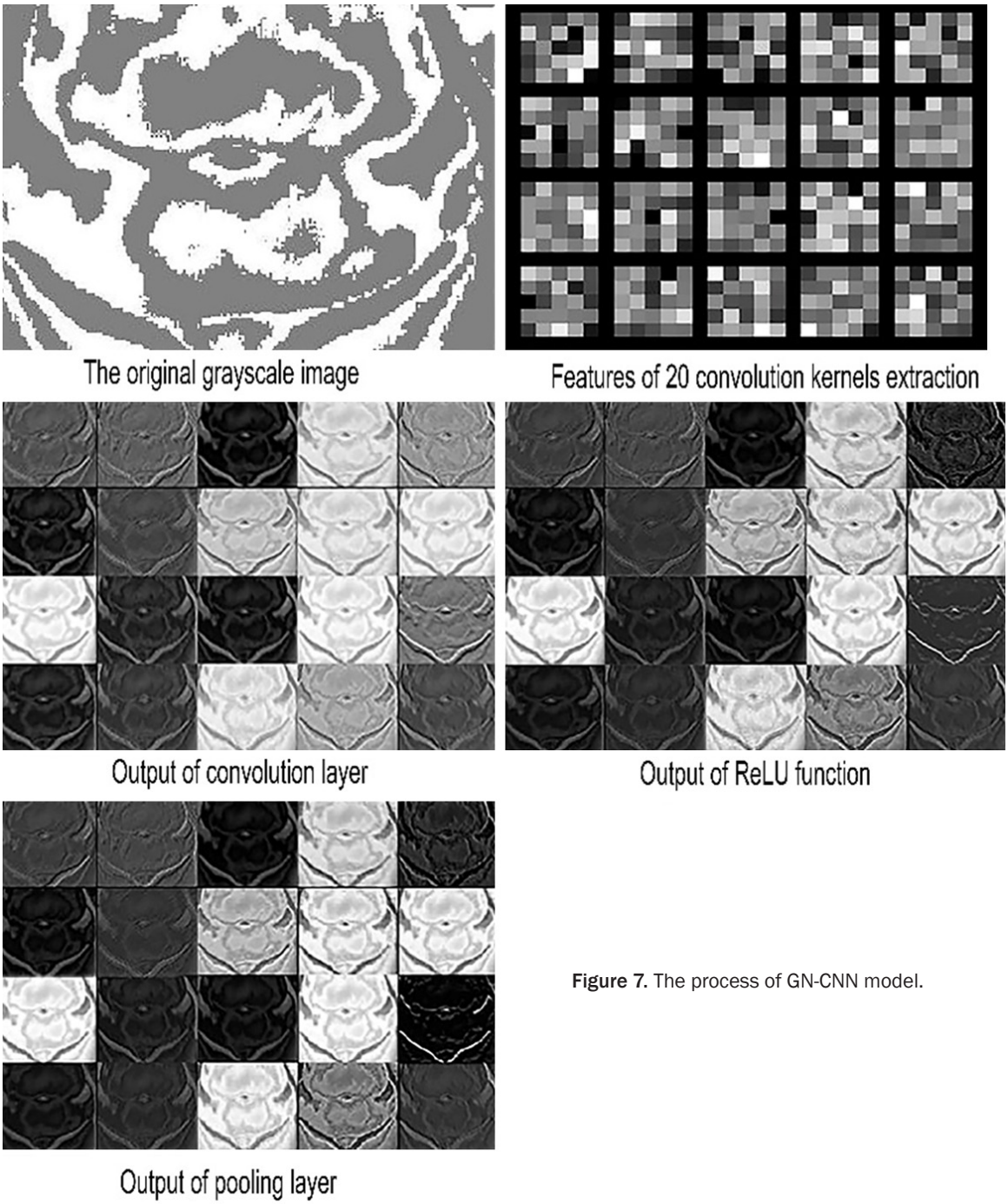


**Figure 7.** The process of GN-CNN model.

**Table 3.** Prediction accuracy based on different models

| | GA-CNN | CNN | DCNN |
|---|---|---|---|
| Colour Image Data Set | 0.8028 | 0.7746 | 0.7888 |
| Gray Image Data Set | 0.9296 | 0.8873 | 0.9155 |

and work to constantly improve the model. In future work, we will consider whole body infrared thermal images of patients comprehensively, examine the correlation between infrared thermal images of different parts of the body, and focus on analysis and prediction from infrared thermal images in the early stage of illness, to ensure that patients can obtain earlier interventions with better outcomes.

In conclusion, this paper proposed a parameter initialization method for a convolution neural network based on a genetic algorithm. The size,

quantity, content of the convolution core and the mode and size of the pooling layer of the convolution neural network were optimized to obtain the optimal network structure, which avoids the influence of random initialization of weight used with traditional neural networks and improves the accuracy of the network. The superiority of the method proposed in this paper was verified by improving the accuracy of the GA-CNN model to 92.96%. The GA-CNN model has very good general abilities and can also be widely used in other pattern recognition problems.

## Acknowledgements

The authors would like to thank National Key R&D Program of China (2018YFC1311900) and the natural science foundation of Shandong province (ZR2018MF006) for the support to this work. In addition, the authors would like to thank people for agreeing to provide data on infrared thermograms.

## Disclosure of conflict of interest

None.

**Address correspondence to:** Longlong Liu, School of Mathematical Sciences at Ocean University of China, Qingdao 266000, P. R. China. Tel: +86-13173237966; Fax: +86-0532-85901752; E-mail: liulonglongmadi@163.com

## References

[1] Ng EY and Kee EC. Advanced integrated technique in breast cancer thermography. J Med Eng Technol 2008; 32: 103-114.

[2] Jesensek Papez B, Palfy M, Mertik M and Turk Z. Infrared thermography based on artificial intelligence as a screening method for carpal tunnel syndrome diagnosis. J Int Med Res 2009; 37: 779-790.

[3] Lahiri BB, Bagavathiappan S, Jayakumar T and Philip J. Medical applications of infrared thermography: a review. Infrared Physics & Technology 2012; 55: 221-235.

[4] Jones BF and Plassmann P. Digital infrared thermal imaging of human skin. Engineering in Medicine & Biology Magazine IEEE 2002; 21: 41-48.

[5] Denoble AE, Hall N, Pieper CF and Kraus VB. Patellar skin surface temperature by thermography reflects knee osteoarthritis severity. Clin Med Insights Arthritis Musculoskelet Disord 2010; 2010: 69-75.

[6] Kacmaz S, Ercelebi E, Zengin S and Cindoruk S. The use of infrared thermal imaging in the diagnosis of deep vein thrombosis. Infrared Physics & Technology 2017; 86: 120-129.

[7] Calin MA, Mologhianu G, Savastru R, Calin MR and Brailescu CM. A review of the effectiveness of thermal infrared imaging in the diagnosis and monitoring of knee diseases. Infrared Physics & Technology 2015; 69: 19-25.

[8] Shih SR, Li HY, Hsiao YL and Chang TC. The application of temperature measurement of the eyes by digital infrared thermal imaging as a prognostic factor of methylprednisolone pulse therapy for graves' ophthalmopathy. Acta Ophthalmol 2010; 88: e154-e159.

[9] Vardasca R and Simoes R. Current issues in medical thermography. 2013.

[10] Lim MJ, Kwon SR, Jung KH, Joo K, Park SG and Park W. Digital thermography of the fingers and toes in Raynaud's phenomenon. J Korean Med Sci 2014; 29: 502.

[11] Liu YL, Tao C, Wang B, Li WZ, Xu GF and Yu B. Application of infrared thermal imaging technology in liquid ammonia storages inspection. American Society of Mechanical Engineers Pressure Vessels & Piping Division Pvp 2014; 1.

[12] Li Z and Zhang X. Application of infrared thermal imaging in the study of preventing cardiovascular and cerebrovascular diseases with Chinese medicine health food. Proc SPIE Int Soc Opt Eng 2009; 7519: 751907-751907-751907.

[13] Wang ZY, Zhang ZF and Jian Y. Infrared technology applied in tongue inspection of traditional Chinese medicine. Journal of Chinese Integrative Medicine 2005; 3: 326.

[14] Zhang JD, HE QH, Sun T, LI HJ, Sun GX and Liu W. Status and prospect of infrared thermal imaging technology applied in TCM researches. China Journal of Traditional Chinese Medicine & Pharmacy 2015.

[15] Ghys R. Comparative value of diaphanoscopy mammography, and thermography for breast cancer screening. 1987.

[16] Li L, Wu SM and Yang TD. Diagnostic value of infrared thermography in vascular diseases. Laser J 2016; 37: 144-147.

[17] Liu L, Qu J, Zhou X, Liu X, Zhang Z, Wang X, Liu T and Liu G. Discovery of a strongly-interrelated gene network in corals under constant darkness by correlation analysis after wavelet transform on complex network model. PLoS One 2014; 9: e92434.

[18] Liu LL, Liu MJ and Ma M. Function clustering self-organization maps (FCSOMs) for mining differentially expressed genes in drosophila and its correlation with the growth medium. Genet Mol Res 2015; 14: 11658-11671.

[19] Liu L, Zhao T, Ma M and Wang Y. A new gene regulatory network model based on BP algorithm for interrogating differentially expressed genes of sea urchin. Springerplus 2016; 5: 1911.
[20] Liu L, Ma M and Cui J. A novel model-based on FCM-LM algorithm for prediction of protein folding rate. J Bioinform Comput Biol 2017; 15: 1750012.
[21] Haberman JAD, Goin JE, Love TJ, Ohnsorg FR and Berry H. Computer techniques In breast cancer detection by absolute temperature thermography. Compsac 79-Computer Software & The IEEE Computer Society 1979.
[22] Jung SKP, Hsieh SJT and Chen CH. Experimental model for determining developmental stage of chicken embryo using infrared images and Artificial neural networks. Spie Defense, Security, & Sensing 2013.
[23] Lessa, Vanessa and Mauricio Marengoni. Applying artificial neural network for the classification of breast cancer using infrared thermographic images. International Conference on Computer Vision & Graphics 2016.
[24] Silva LF, Saade DCM, Sequeiros GO, Silva AC, Paiva AC, Bravo RS and Conci A. A new database for breast research with infrared image. Journal of Medical Imaging and Health Informatics 2014; 4: 92-100.
[25] Koay J, Herry C and Frize M. Analysis of breast thermography with an artificial neural network. International Conference of The IEEE Engineering in Medicine and Biology Society 2005.
[26] Jin C, Yang Y, Xue ZJ, Liu KM and Liu J. Automated analysis method for screening knee osteoarthritis using medical infrared thermography. Journal of Medical & Biological Engineering 2013; 33: 471-477.